Journal of Membrane Science 732 (2025) 124270

Contents lists available at ScienceDirect

Journal of Membrane Science

journal homepage: www.elsevier.com/locate/memsci

Time-evolved growth of semi-aromatic polyamide nanofilms and their structure-performance relationship: Mechanistic insights and implications for nanofiltration membrane synthesis

Shenghua Zhou [a], Zhuting Wang [a], Wenyu Liu [a], Yaowen Hu [a], Ke Jiang [a], Lu Elfa Peng [a,*], Hao Guo [b,c], Chuyang Y. Tang [a,**]

[a] Department of Civil Engineering, The University of Hong Kong, Pokfulam, 999077, Hong Kong Special Administrative Region of China
[b] Institute of Environment and Ecology, Shenzhen International Graduate School, Tsinghua University, Shenzhen, 518055, PR China
[c] Guangdong Provincial Key Laboratory of Carbon Fixation and Sinks, Department of Education of Guangdong Province, Shenzhen International Graduate School, Tsinghua University, Shenzhen, 518055, PR China

ARTICLE INFO

Keywords:
Semi-aromatic polyamide film
Growth kinetics
Film thickness
Asymmetric structures
Separation performance

ABSTRACT

The separation performance of thin film composite nanofiltration (NF) membranes is governed by a semi-aromatic polyamide film. Compared to fully aromatic polyamide films with a well-known self-limiting behavior, the growth kinetics of semi-aromatic polyamide films and the corresponding regulation mechanisms have not been fully understood. This study systematically investigated the time-evolved growth of a piperazine (PIP)-based polyamide film at a free interface over prolonged interfacial polymerization reaction time (up to 60 min). For the first time, we revealed a two-stage growth kinetics, with the film growth rate in the later stage (7.0 nm min^{-1}) one order of magnitude slower than the initial rate (68.2 nm min^{-1}) as a result of reduced availability of PIP monomers. This two-stage growth mechanism led to an asymmetric film structure, with compelling characterization results (i.e., crosslinking degree, film density, and pore size) showing that the newly formed polyamide under the reduced PIP availability was much looser than the incipient film. We demonstrated that such asymmetric structure had profound impact on the separation performance of the resulting NF membrane through mechanisms such as internal concentration polarization and gutter effect. The mechanistic insights into the growth-structure-performance relationship of semi-aromatic polyamide films could guide the synthesis of high-performance NF membranes.

1. Introduction

Polyamide thin film composite (TFC) membranes have been widely adopted by nanofiltration (NF) and reverse osmosis (RO) for contaminant removal and freshwater production to address global water scarcity [1–3]. Over the past decades, they have increasingly dominated desalination capacity with approximately 74 % of the current desalination plants utilizing polyamide-based membrane separation technology [4]. A typical polyamide film is synthesized by interfacial polymerization (IP) at an interface between amine monomers in water and acyl chloride monomers in organic solvents. Traditional wisdom believes that the formation of a polyamide film is fast and self-terminated [5–9]. For example, Chai [7] reported that the IP reaction could be almost completed within 20 s, as evidenced by a rapid initial increase in film thickness followed by a plateau over extended reaction time of 5 min. This experimental observation of self-limiting growth was also confirmed by several other groups [8,9]. Notably, many of these studies focused on fully-aromatic polyamide films [7–9] that are prepared by *m*-phenylenediamine (MPD) and trimesoyl chloride (TMC)–a standard recipe for RO membranes. Such membranes typically present a molecular weight cut-off (MWCO) of ~ or < 100 Da [10,11], which would restrict further diffusion of MPD monomers (MW of 108 Da) and thus terminate the IP reaction after the rapid formation of an incipient polyamide film.

Despite the increasing demands for NF membranes in various practical applications [12,13], limited studies have been documented for the

* Corresponding author.
** Corresponding author.
E-mail addresses: elfapeng@connect.hku.hk (L.E. Peng), tangc@hku.hk (C.Y. Tang).

https://doi.org/10.1016/j.memsci.2025.124270
Received 12 April 2025; Received in revised form 17 May 2025; Accepted 25 May 2025
Available online 26 May 2025

time-evolved growth of semi-aromatic polyamide films. Theoretically, the self-limiting mechanism documented for RO membranes may not be readily extended to semi-aromatic polyamide NF membranes considering the largely different amine monomer properties and polyamide film structures. Specifically, semi-aromatic polyamide films, prepared by a lower-reactivity amine monomer piperazine (PIP) [14], present a looser film structure [6,15] with typical MWCOs in the range of 100–500 Da [16,17]. At the same time, PIP monomers have a small MW of 86 Da. During the IP reaction, these small amine monomers may easily penetrate through the incipient polyamide film, allowing their continuous reaction with TMC monomers. Therefore, we hypothesize that PIP-based semi-aromatic polyamide films will grow continuously over extended reaction time, in contrast to the self-limiting behavior of fully-aromatic ones. This difference in the growth mechanism may greatly influence the physicochemical properties of NF membranes, which could further impact the mass transport through the polyamide film and thereby determine membrane separation performance.

This study aims to systematically investigate the growth mechanism of semi-aromatic polyamide. A series of polyamide films were fabricated at increasing reaction time (i.e., 0.5 min, 1 min, 5 min, 10 min, and 60 min) to reveal the evolution of polyamide film growth. To ensure a sufficient supply of PIP monomers for polyamide growth over an extended duration, a support-free IP strategy was adopted. We further characterized the properties such as thickness and crosslinking degree of these films and evaluated their impacts on separation performance. The in-depth understanding of the time evolution of the film structure and the relevant separation properties provides crucial guidance for the design and synthesis of semi-aromatic polyamide films.

2. Materials and methods

2.1. Chemicals

Piperazine (PIP, 99 %), trimesoyl chloride (TMC, 98 %), and *n*-hexane (95 %) were purchased from Sigma-Aldrich to synthesize polyamide films by an IP reaction. A range of neutral solutes with increasing MW, including glycerol (MW: 92 g mol^{-1}, 99.7 %, Dieckmann), pentaerythritol (MW: 136 g mol^{-1}, 99.7 %, Dieckmann), Glucose (MW: 180 g mol^{-1}, 99.7 %, Uni-Chem) and sucrose (MW: 342 g mol^{-1}, 99.7 %, Dieckmann), were chosen for evaluating MWCOs and pore sizes of polyamide films. Silver nitrate ($AgNO_3$, ≥99.0 %, Sigma-Aldrich) and nitric acid (HNO_3, 69 %, trace metals basis, VWR) were purchased to analyze the density of charged carboxyl groups and ion accumulation in the polyamide films. Sodium sulfate (Na_2SO_4, 99.7 %, Dieckmann) was utilized to evaluate film separation performance. Unless otherwise stated, all aqueous solutions in this study were prepared using ultrapure water from a Millipore Integral 10 Water Purification System with a resistivity of 18.2 MΩ cm.

2.2. Fabrication of polyamide films via a support-free IP strategy

A series of polyamide films were fabricated by a support-free IP method [18–20] (Fig. S2) between PIP (dissolved in water) and TMC (dissolved in *n*-hexane) with increasing reaction time (i.e., 0.5, 1, 5, 10, and 60 min, respectively). Firstly, 0.1 wt% PIP solution was poured into a lab-made container (Fig. S3) with a polyethersulfone (PES) substrate (Microdyn Nadi, MWCO: 150 kDa) preloaded (Fig. S2). Subsequently, 0.05 wt% TMC solution was carefully added on the surface of PIP solution by a pipette to synthesize polyamide films. In this study, the surface of a polyamide film exposed to the organic phase during the IP reaction was defined as the front side. Conversely, the opposing surface, exposed to the aqueous phase during the IP reaction, was designated as the back side. The fabricated nanofilms with different orientations (front side facing up vs. back side facing up) were deposited on the PES substrate with the assistance of vacuum filtration (Fig. S2) for further characterizations and performance tests [8,18]. The resultant membrane comprising a polyamide film and a PES substrate was named as NF-x, where x denotes the IP reaction time (min).

2.3. Fabrication of conventional TFC membranes

We also fabricated conventional TFC polyamide membranes by conducting IP reactions between PIP (dissolved in water) with different concentrations (i.e., 0.1 and 1 wt%) and 0.05 wt% TMC (dissolved in *n*-hexane) on the PES substrate. Briefly, the porous PES substrate was soaked into a PIP solution for 2 min and the excess PIP solution was removed by a rubber roller. The TMC solution was then gently poured onto the PIP-impregnated PES substrate for 0.5 or 5 min to synthesize the polyamide membrane. The formed TFC membrane was thoroughly rinsed by *n*-hexane to remove unreacted TMC monomers. The resultant membranes were named as TFC-x (for 0.1 wt% PIP) or TFC-xH (for 1 wt % PIP), with the letter x referring to IP reaction time (0.5 and 5 min).

2.4. Characterization of the polyamide films

The surface morphology of a polyamide film was resolved by a scanning electron microscope (SEM, S-4800, Hitachi) with an accelerating voltage of 5 kV. Before the SEM characterization, all polyamide films were dried in an oven at 40 °C overnight and then coated with a thin gold layer by a turbomolecular pumped coater (Q150T ES Plus, Quorum) to increase sample conductivity. Film cross-sectional structures were characterized by a transmission electron microscope (TEM, G2, FEI Tecnai). An atomic force microscope (AFM, Dimension 3100, Vecco) with a scan rate of 6 Hz was used to measure surface roughness (i.e., root-mean-square roughness, *Rq*) and film thickness. The areal mass of polyamide films was measured by a quartz crystal microbalance (QCM, Q-Sense E4, Biolin Scientific), which can be further adopted to calculate film density together with AFM thickness results (**Supplementary materials**, **Section S8**) [21–23]. The functional groups of polyamide films were analyzed by an attenuated total reflectance Fourier transform infrared spectroscopy (ATR-FTIR, Nicolet IS5, Thermo Fisher Scientific) with wavenumber ranging from 800 to 2000 cm^{-1}. The elemental contents of a polyamide film were detected by an X-ray photoelectron spectroscope (XPS, Axis Ultra DLD), and the crosslinking degree (*n*) of polyamide films can be calculated based on the obtained O/N ratio (*r*) following the equation: $n = (4\text{-}2r)/(1 + r)$ [21].

2.5. Evaluation of separation performance

A lab-scale crossflow filtration setup was used to test film separation performance at room temperature of ~25 °C. The fabricated polyamide membranes were installed into parallel crossflow cells with an effective filtration area of 2 cm^2, with either the front side or the back side of the polyamide films facing the feed solution. The film samples were precompacted with 1 L feed solution (i.e., DI water, 1 g L^{-1} Na_2SO_4 solutions, 0.2 g L^{-1} neutral molecular solutions, or 1 g L^{-1} PIP solution) at 5 bar with a crossflow velocity of 16.7 cm s^{-1} for 1 h before collecting permeate solutions. Water flux (J_v, L m^{-2} h^{-1}), water permeance (A, L m^{-2} h^{-1} bar^{-1}), and solute rejection (R, %) can be calculated by

$$J_v = \frac{\Delta m}{\rho \times a \times \Delta t} \tag{1}$$

$$A = \frac{J_v}{\Delta P - \Delta \pi} \tag{2}$$

$$R = \frac{C_f - C_p}{C_f} \times 100\% \tag{3}$$

where Δm (g) is the mass of the permeate solution collected throughout Δt (h), ρ (g cm^{-3}) is the density of permeate water, ΔP (bar) is the applied pressure, $\Delta \pi$ (bar) is the transmembrane osmotic pressure, C_f and C_p are the concentrations of the feed solution and the permeate

solution, respectively. The concentrations of salt ions were measured directly using a portable conductivity meter (Myron II, Myron L). Concentrations of neutral molecules and PIP monomers were analyzed by a total organic carbon (TOC) analyzer (TOC-L CPH, SHIMADZU).

3. Results and discussion

3.1. Roughness of polyamide films

As shown in Fig. 1, an obvious change of surface morphology was observed for polyamide films fabricated over different IP reaction time (from 0.5 to 60 min). Specifically, the IP reaction time of 0.5 min (NF-

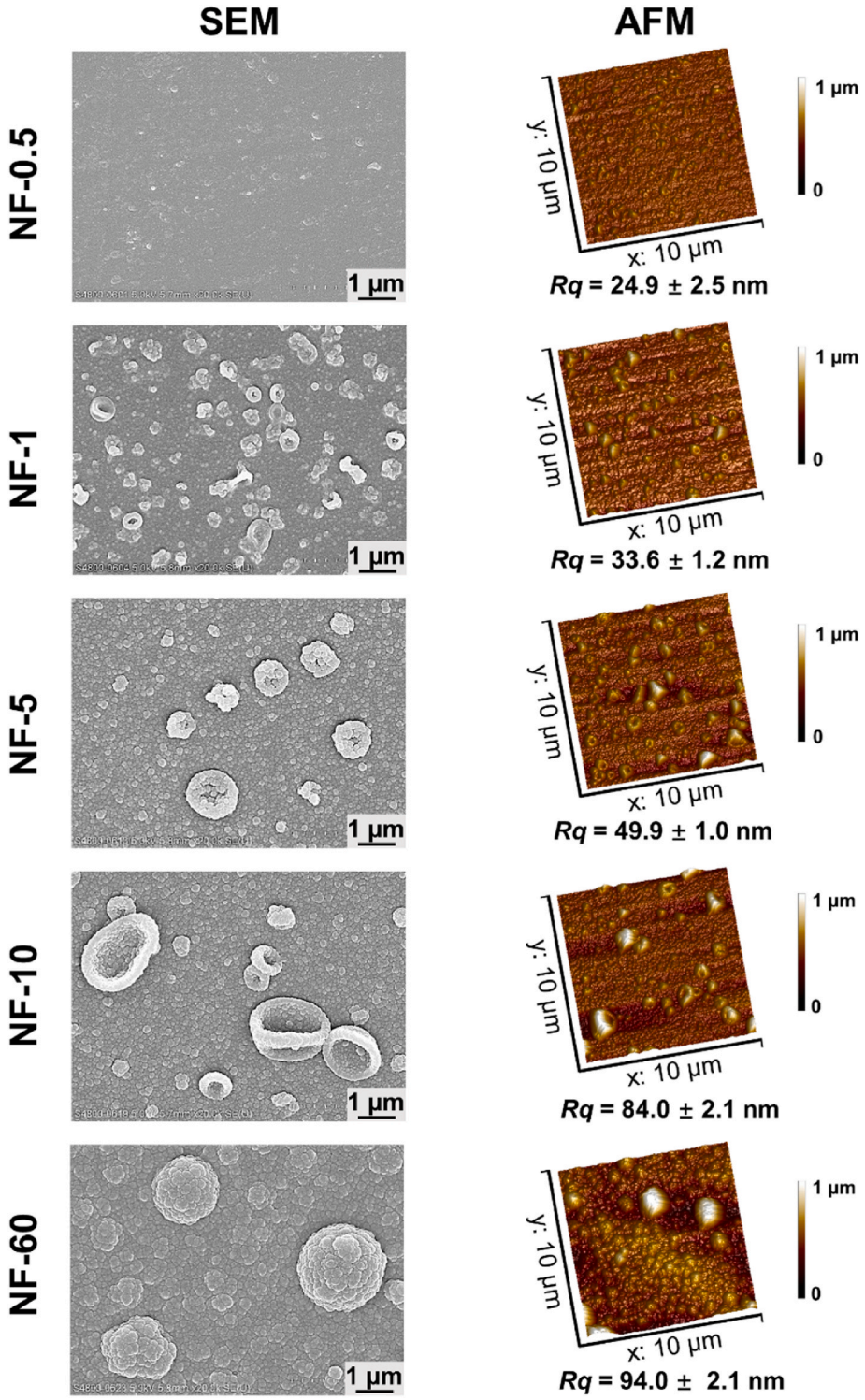

Fig. 1. Microscopic characterizations by SEM (top view) and AFM for the front side of polyamide films formed at different reaction time (0.5–60 min). In the AFM images, *Rq* is the root-mean-square roughness. The error bars represent the standard deviation based on at least three measurements for independent polyamide films.

0.5) resulted in a relatively smooth film surface, which is consistent with the previous reports [9,18,24,25]. Prolonging the IP reaction time led to the formation of increasingly larger nodular structures. Consistently, their surface roughness (*Rq*, root-mean-square roughness) quantified by AFM increased from 24.9 nm for NF-0.5 to 94.0 nm for NF-60.

3.2. Thickness of polyamide films

To better reveal the evolution of polyamide film growth, we further characterized the thickness of polyamide films formed at different IP reaction time by AFM height profile measurements (Fig. 2a and b). As expected, longer reaction time led to continuous growth in polyamide film thickness (from 33.4 nm for NF-0.5 to 486.7 nm for NF-60). The AFM thickness results were further confirmed by TEM cross-sectional characterization (Fig. 2c1-c5). These results indicate that PIP monomers could penetrate through the polyamide film to react with TMC monomers continuously. This observation was further supported by the PIP passage tests (Fig. S6) that a substantial fraction of PIP can still penetrate through the polyamide film even at the IP reaction time of 60 min. The increased film thickness with prolonged reaction was also observed for semi-aromatic polyamide in previous studies [9,26], although these studies adopted relatively short reaction durations (e.g., 3 min) that limited further analysis for film growth kinetics.

Interestingly, in this study, two-stage kinetics were observed for the growth of semi-aromatic polyamide films (Fig. 2b). The film thickness increased rapidly at the rate of 68.2 nm min^{-1} within the first minute, which was followed by a much slower growth afterward (i.e., 7.0 nm min^{-1}). Despite the greatly reduced growth rate, the polyamide film continued to grow over extended reaction time. This growth behavior was dramatically different from that of fully-aromatic polyamide. For the latter, its film thickness almost leveled off (growth rate <0.1 nm min^{-1}) after a rapid film formation within the first 0.5 min [8]. The two-stage growth of semi-aromatic polyamide could be attributed to the varied PIP monomer availability. In the initial stage, the high availability of PIP enables the rapid formation of an incipient polyamide film. However, this incipient polyamide film slows down further diffusion of PIP monomers, leading to reduced availability of monomers (Fig. S6) and slower film growth (Fig. 2b). This observation is consistent with the analytical model proposed by Freger [5], which describes a two-stage polyamide film growth governed by monomer diffusion. According to this model, polyamide has a nearly constant growth rate in the initial stage since the *trans*-interface PIP diffusion remained largely unchanged. According to the author, once the incipient film is formed, the resistance for PIP diffusion could be increased by orders of magnitude, leading to greatly reduced PIP supply for further film growth.

3.3. Crosslinking degree and density of polyamide films

Notably, TEM images show an obvious difference in relative darkness between the front and back sides for polyamide films formed at long reaction time (i.e., NF-10 and NF-60, Fig. 2c), indicating an asymmetric structure of these films. According to previous studies [27,28], such difference in darkness can be attributed to the variation in the relative mass density, with darker color indicating denser polyamide. Consistent with the much darker color of the back sides shown in TEM images, the back sides also had higher crosslinking degrees than the front sides (Fig. 3a). Indeed, for all films formed at different IP reaction time, similar crosslinking degrees were observed for the back sides. This could be explained by the fact that the back side of a polyamide film, exposed to the aqueous phase, is formed in the initial stage of the IP reaction. The high PIP availability during this stage [29] ensures the formation of highly crosslinked incipient films (over 70 %) with similar quality. To further verify the property similarity of the incipient polyamide films, we performed filtration tests by exposing their back sides to the feed solution containing 0.2 g L^{-1} neutral molecules to analyze their MWCOs and pore sizes (Fig. 3b). As expected, all the films exhibited nearly identical MWCO (~137 Da) and pore radius (r_p, ~0.26 nm). Compared to the back sides, the front sides (facing the organic phase) had greatly reduced crosslinking degree (Fig. 3a), higher MWCO, and larger pore sizes (Fig. S7), particularly for films formed at long reaction time (e.g., NF-60). These trends can be attributed to the declined PIP availability upon the formation of the dense incipient film, which subsequently resulted in a loose structure for the front side. For MWCO evaluation with the front side facing the feed solution, the neutral solutes could

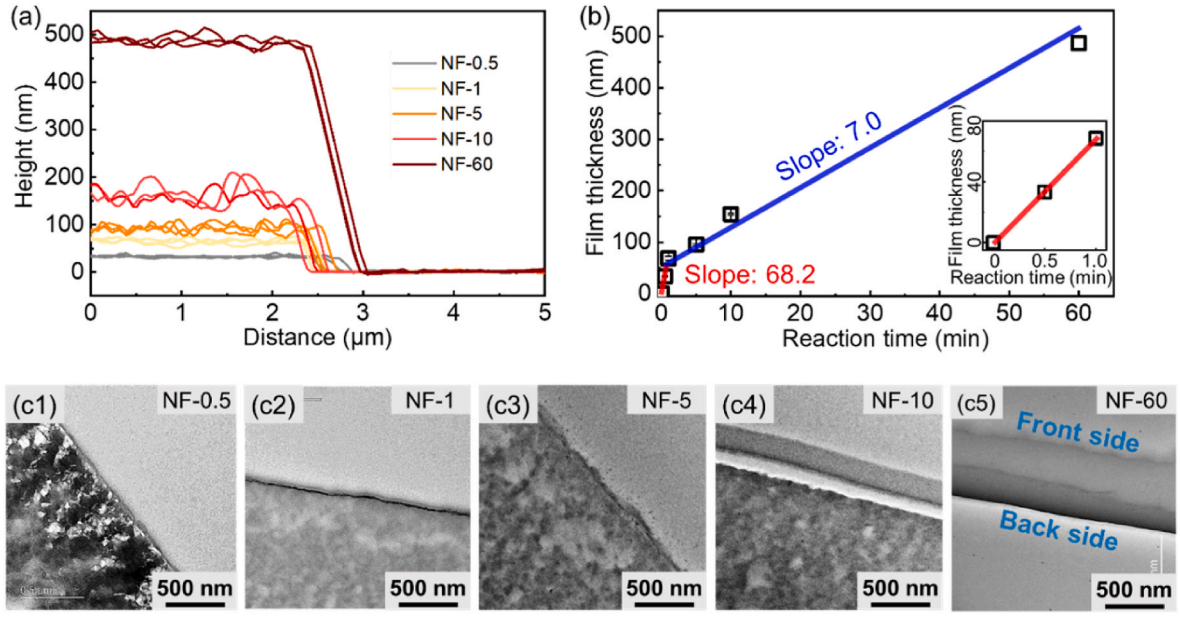

Fig. 2. (a) AFM height profiles of polyamide nanofilms formed at 0.5–60 min. (b) Evolution of polyamide film thickness over time. The insert shows the growth of film thickness within the first minute. (c1-c5) TEM micrographs of polyamide nanofilms formed at 0.5–60 min. The AFM height profiles were obtained by transferring polyamide films onto silicon wafers before AFM characterization. Polyamide film thickness was obtained based on the AFM results and three different areas of each film sample were measured. For part (b), the size of error bar was smaller than the size of the symbol. (For interpretation of the references to color in this figure legend, the reader is referred to the Web version of this article.)

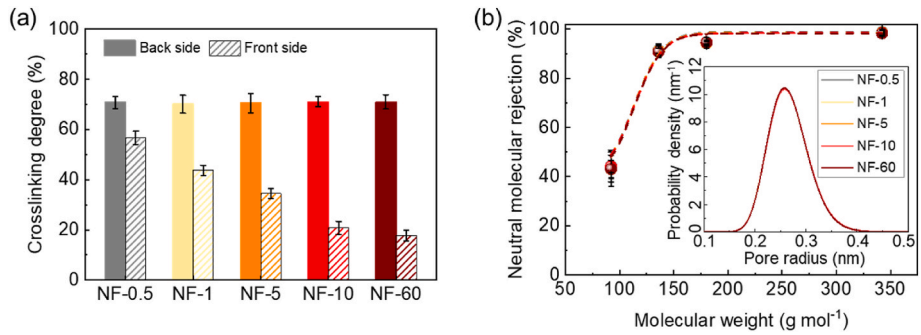

Fig. 3. (a) The crosslinking degree of the back side (i.e., exposed to the aqueous phase during the IP reaction) and the front side (i.e., facing the organic phase during the IP reaction) of polyamide films formed at different reaction time (b) Rejection of four neutral molecules (i.e., glycerol, pentaerythritol, glucose, and sucrose) by polyamide films formed at different reaction time. During the filtration tests, the back side of the polyamide films was exposed to the feed solution. The inset was the pore size distribution of polyamide films obtained based on rejection results of neutral molecules (see detailed calculation in **Supplementary materials, Section S6**). The error bars represent the standard deviation based on at least three measurements for independent polyamide films.

easily penetrate the loose front side but were retained by the dense back side. The solute accumulation within the polyamide film, a form of internal concentration polarization (ICP) [30], could increase effective solute concentration close to the dense back side, resulting in lower solute rejections and thus a larger experimental MWCO value. In contrast, the ICP phenomenon could be mitigated with the dense surface facing the feed solution, contributing to higher rejection and smaller MWCO. Accordingly, the density of charged carboxyl groups increased with extended reaction time (Fig. S8). This can be attributed to the suppressed PIP availability by the incipiently formed dense layer, which reduces the crosslinking of the subsequently formed polyamide and results in more unreacted acyl chloride groups of TMC. These unreacted acyl chloride groups could be then hydrolyzed to negatively charged carboxyl groups.

We further conducted QCM characterization to evaluate the areal mass of the polyamide films (Fig. S9) [8,31,32]. Together with the film thickness results (Fig. 2a and b), polyamide film density (Fig. S10) can be quantified (see detailed calculation in Supplementary materials, Section S8). For short reaction time up to 1 min, the semi-aromatic polyamide films had similar densities (1.17 g cm^{-3} for NF-0.5 and 1.14 g cm^{-3} for NF-1). These values are slightly lower than those of fully-aromatic polyamide films (1.24–1.28 g cm^{-3}) [8], in good agreement with the larger effective pore sizes of NF membranes [33,34]. In the current study, the overall density of the semi-aromatic polyamide films significantly reduced at longer reaction time (e.g., 1.05 g cm^{-3} for NF-5). Assuming a similar density for all the back sides (which is well supported by their similar crosslinking degree, Fig. 3a), this result implies that the subsequently formed polyamide on the front side had a greatly lower density (with an average value of 0.81 g cm^{-3} during 1–5 min, Fig. S10).

Combining the above results of the two-stage thickness growth (Fig. 2b) and asymmetric density evolution of the semi-aromatic polyamide film (Fig. S10), we illustrate a time-evolved formation process in Fig. 4. During the initial IP reaction, the high availability of PIP monomers resulted in a greatly crosslinked incipient film featuring high density and relatively small pore size. This incipient film would suppress the subsequent *trans*-film monomer diffusion and reduce PIP availability for the subsequent growth of front-side polyamide, leading to an asymmetric polyamide film structure with a denser back side and a looser front side.

3.4. Separation performance of polyamide films

We performed filtration tests to evaluate the separation performance of the polyamide films by exposing their front sides or back sides to a feed solution containing 1 g L^{-1} Na_2SO_4. The back side filtration (back side facing up) showed a comparable Na_2SO_4 rejection (Fig. 5a), which is consistent with the similar crosslinking degree (Fig. 3a). In contrast, the front side filtration (front side facing up) presented a declined rejection from 99.0 % to 88.0 % when increasing the IP duration from 0.5 to 60 min (Fig. 5a). For a film with an asymmetric structure (NF-5 or NF-60), the front side rejection was lower than the corresponding back side rejection. This difference became more pronounced for NF-60. At the same time, water flux obtained from front side filtration was lower than the corresponding value for the back side filtration, with a flux ratio of as high as 3.0 for NF-60 (Fig. 5b). These peculiar phenomena can be partially attributed to the more severe ICP for the front side filtration (Fig. 5c). When the less crosslinked front side is exposed to the feed solution, solutes can easily enter this loose layer, but they will be retained by the dense back side layer, leading to their accumulation within the polyamide film. This ICP phenomenon, which occurs inside the polyamide film and is somewhat analogous to ICP in forward osmosis [35,36], causes higher effective solute concentration and elevated osmotic pressure for the front side filtration. In contrast, this unfavorable ICP does not occur for the back side filtration, such that the latter film orientation presents both higher solute rejection and better water flux. An added advantage for the back side filtration is that a relatively loose polyamide layer is sandwiched between a denser

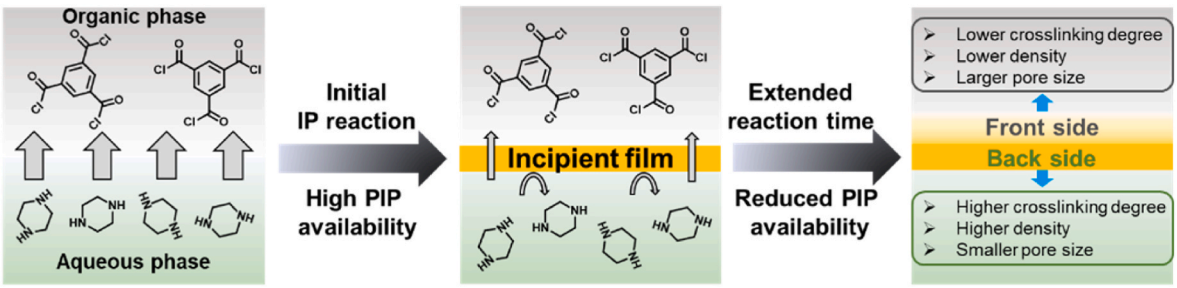

Fig. 4. Schematic diagram of the growth of a semi-aromatic polyamide film with an asymmetric structure.

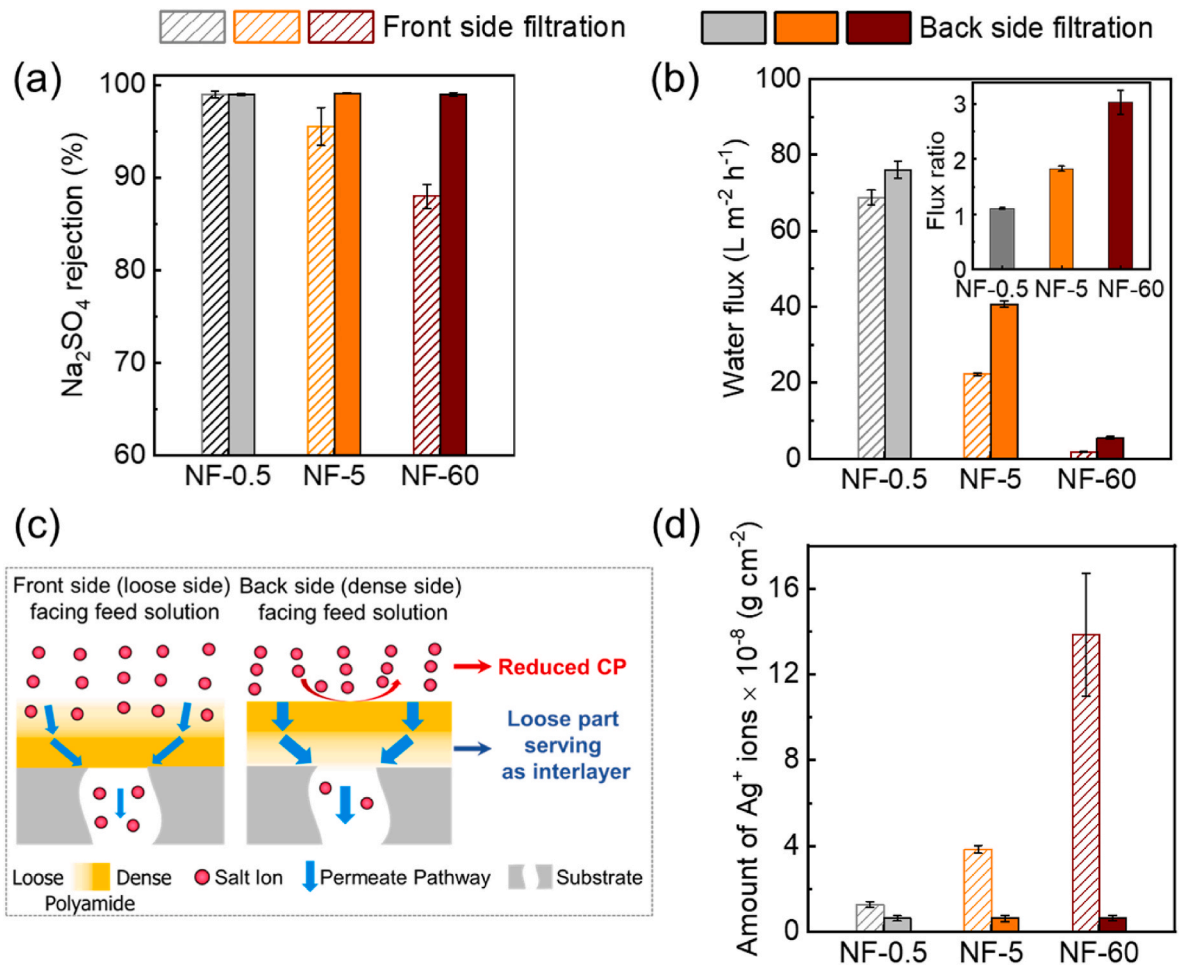

Fig. 5. (a) Na_2SO_4 rejection and (b) water flux of the polyamide films, with either the front side or the back side of the polyamide films facing the feed solution (i.e., 1 g L^{-1} Na_2SO_4). The inset in part (b) presents the ratio of flux values (back side filtration over front side filtration). (c) Schematic diagram of front side filtration (front loose side facing up) vs. back side filtration (back dense side facing up). (d) The amount of Ag^+ ions present inside the polyamide films after filtration of a 10 μM $AgNO_3$ solution in front side and back side filtration. Each filtration test was performed for 1 h with an applied pressure of 5 bar. After the filtration test, the polyamide film was immersed in a 1 % HNO_3 solution for 30 min to leach the bound silver ions, while the Ag^+ concentration was analyzed by an inductively coupled plasma mass spectrometry. The error bars represent the standard deviation based on at least three measurements for independent polyamide films.

polyamide layer and the porous substrate, leading to a beneficial gutter effect [37] (Fig. 5c) analogous to that for interlayered TFC membranes [38–41]. A simple model was further employed to demonstrate this beneficial effect (Fig. S12). Specifically, the loose layer on the bottom can serve as a low-hydraulic-resistance gutter [37,42,43] (Fig. S12a) to shorten the transport path length in the dense part, leading to reduced overall hydraulic resistance in the polyamide film. In contrast, when the dense part is on the bottom, a severe funnel-like transport pattern occurs inside this less-permeable dense layer (Fig. S12b). This unfavorable "funnel effect" is known to drastically increase the overall hydraulic resistance and reduce membrane transport efficiency [37,44,45].

To further confirm the ICP, we filtered an $AgNO_3$ solution (10 μM) through the polyamide films in the two different film orientations. The Ag^+ ions bound inside the polyamide films were subsequently leached by HNO_3 [46]. For NF-60 (with the most pronounced asymmetric structure), the leached Ag^+ concentration for the front side filtration was more than an order of magnitude higher than that for the back side filtration (Fig. 5d). These results indicate a higher tendency of ICP for the front side filtration.

3.5. Perspective

For practical fabrication of TFC NF membranes, the IP reaction is performed directly on a porous substrate instead of at a free interface. Therefore, we further prepared conventional TFC semi-aromatic polyamide membranes on a PES substrate using two different reaction time (0.5 and 5 min). With a high PIP concentration of 1 wt%, prolonged reaction time from 0.5 to 5 min also led to a simultaneous reduction in both water permeance and Na_2SO_4 rejection (TFC-0.5H and TFC-5H, Fig. 6). However, using a lower PIP concentration of 0.1 wt%, longer reaction time appears to be beneficial for boosting Na_2SO_4 rejection from 95.0 % to 99.2 % (TFC-0.5 and TFC-5). For the latter case, the lower PIP concentration could cause a looser incipient film, which allows PIP monomers to continuously diffuse through and suppress the formation of undesirable asymmetric structures. Future studies may further explore strategies for creating "inversed asymmetric structures" featuring a dense front surface atop a loose back surface. For example, one may adopt large-MW amine monomers with low concentration to form a loose incipient polyamide film, followed by the use of small-MW amine monomers (which minimizes the retardation by the incipient film) to create a dense front surface. Monomers with different reactivities [47] may also be used to further optimize such "inversed asymmetric structures". Alternatively, layer-by-layer IP [48] or electrospray-based additive IP [49,50] may be programmed to create polyamide structures with desired gradient of crosslinking degree.

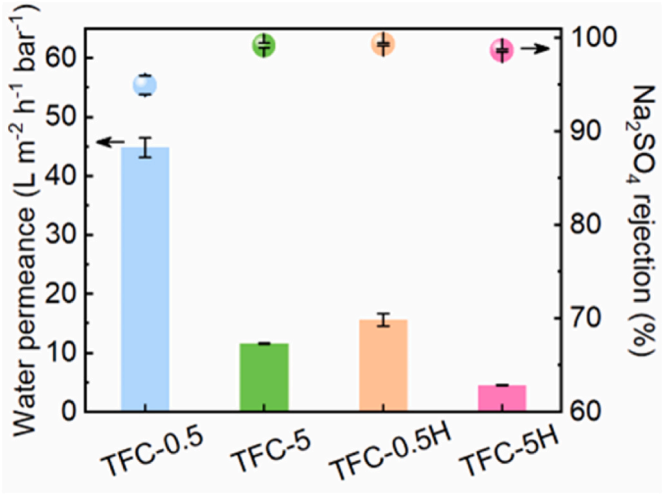

Fig. 6. Water permeance and Na_2SO_4 rejection of TFC semi-aromatic polyamide membranes by conducting conventional IP reaction on a porous PES substrate with different reaction time (0.5 and 5 min). The resultant membranes were named as TFC-x (for 0.1 wt% PIP) or TFC-xH (for 1 wt% PIP), with the letter x referring to IP reaction time (0.5 and 5 min). The error bars represent the standard deviation based on at least three measurements for independent polyamide films.

4. Conclusions

In the current study, we deciphered the structural evolution of semi-aromatic polyamide films over extended IP reaction time. In contrast to the traditional wisdom, the growth of semi-aromatic polyamide films shows a two-stage kinetics instead of self-limiting behavior. Initially high PIP availability allows the fast growth of incipient polyamide film with a relatively high mass density (1.17 g cm^{-3}). This dense incipient film retards the subsequent PIP supply, which slows down the growth kinetics and forms a looser polyamide structure toward the front side. Long IP reaction time leads to a thick polyamide film with greatly increased hydraulic resistance. This thick film also features an asymmetric structure with a loose front surface and a dense back side, which is prone to severe ICP when tested in front side filtration. As a result, excessively long IP reaction time could cause a simultaneous reduction in both water flux and salt rejection, which should be strictly avoided. We demonstrate better separation performance for the back side filtration that suppresses ICP and promotes gutter effect. The critical mechanistic insights for the growth kinetics and structure-performance relationships would provide important guidance for the future design and optimization of semi-aromatic polyamide membranes.

CRediT authorship contribution statement

Shenghua Zhou: Writing – original draft, Methodology, Investigation, Formal analysis, Data curation, Conceptualization. **Zhuting Wang:** Methodology, Formal analysis. **Wenyu Liu:** Methodology, Formal analysis. **Yaowen Hu:** Formal analysis. **Ke Jiang:** Formal analysis. **Lu Elfa Peng:** Writing – review & editing, Formal analysis. **Hao Guo:** Formal analysis, Conceptualization. **Chuyang Y. Tang:** Writing – review & editing, Supervision, Resources, Project administration, Funding acquisition, Formal analysis, Data curation.

Declaration of competing interest

The authors declare that they have no known competing financial interests or personal relationships that could have appeared to influence the work reported in this paper.

Acknowledgments

This work was substantially supported by grants from the Research Grants Council of the Hong Kong Special Administration Region, China (SRFS2021-7S04 and GRF 17201921). This work was also partially supported by the Seed Fund for Strategic Interdisciplinary Research Scheme (102010174) from The University of Hong Kong. The QCM characterizations were supported by the URC Small Equipment Fund (102010138) and the Seed Fund for Basic Research (202011159093) from The University of Hong Kong. We appreciated the Electron Microscopic Unit (EMU) at The University of Hong Kong for SEM and TEM sample preparation and characterization.

Appendix A. Supplementary data

Supplementary data to this article can be found online at https://doi.org/10.1016/j.memsci.2025.124270.

Data availability

Data will be made available on request.

References

[1] M. Elimelech, W.A. Phillip, The future of seawater desalination: energy, technology, and the environment, Science 333 (6043) (2011) 712–717, https://doi.org/10.1126/science.1200488.
[2] J.R. Werber, A. Deshmukh, M. Elimelech, The critical need for increased selectivity, not increased water permeability, for desalination membranes, Environ. Sci. Technol. Lett. 3 (4) (2016) 112–120, https://doi.org/10.1021/acs.estlett.6b00050.
[3] X. Lu, M. Elimelech, Fabrication of desalination membranes by interfacial polymerization: history, current efforts, and future directions, Chem. Soc. Rev. 50 (11) (2021) 6290–6307, https://doi.org/10.1039/D0CS00502A.
[4] N. Voutchkov, Striving for Desalination's Gold Sustainability Standard, International Water Association, 2023. December 31.
[5] V. Freger, Kinetics of film formation by interfacial polycondensation, Langmuir 21 (5) (2005) 1884–1894, https://doi.org/10.1021/la048085v.
[6] V. Freger, G.Z. Ramon, Polyamide desalination membranes: formation, structure, and properties, Prog. Polym. Sci. 122 (2021) 101451, https://doi.org/10.1016/j.progpolymsci.2021.101451.
[7] G.-Y. Chai, W.B. Krantz, Formation and characterization of polyamide membranes via interfacial polymerization, J. Membr. Sci. 93 (2) (1994) 175–192, https://doi.org/10.1016/0376-7388(94)80006-5.
[8] S. Zhou, L. Long, Z. Yang, S.L. So, B. Gan, H. Guo, S.-P. Feng, C.Y. Tang, Unveiling the growth of polyamide nanofilms at water/organic free interfaces: toward enhanced water/salt selectivity, Environ. Sci. Technol. 56 (14) (2022) 10279–10288, https://doi.org/10.1021/acs.est.1c08691.
[9] C. Jiang, L. Zhang, P. Li, H. Sun, Y. Hou, Q.J. Niu, Ultrathin film composite membranes fabricated by novel in situ free interfacial polymerization for desalination, ACS Appl. Mater. Interfaces 12 (22) (2020) 25304–25315, https://doi.org/10.1021/acsami.0c05166.
[10] C. Li, Y. Zhao, G.S. Lai, R. Wang, Fabrication of fluorinated polyamide seawater reverse osmosis membrane with enhanced boron removal, J. Membr. Sci. 662 (2022) 121009, https://doi.org/10.1016/j.memsci.2022.121009.
[11] H.K. Shon, S. Vigneswaran, J. Cho, Comparison of physico-chemical pretreatment methods to seawater reverse osmosis: detailed analyses of molecular weight distribution of organic matter in initial stage, J. Membr. Sci. 320 (1) (2008) 151–158, https://doi.org/10.1016/j.memsci.2008.03.063.
[12] A.W. Mohammad, Y.H. Teow, W.L. Ang, Y.T. Chung, D.L. Oatley-Radcliffe, N. Hilal, Nanofiltration membranes review: recent advances and future prospects, Desalination 356 (2015) 226–254, https://doi.org/10.1016/j.desal.2014.10.043.
[13] H. Guo, X. Li, W. Yang, Z. Yao, Y. Mei, L.E. Peng, Z. Yang, S. Shao, C.Y. Tang, Nanofiltration for drinking water treatment: a review, Front. Chem. Sci. Eng. 16 (5) (2022) 681–698, https://doi.org/10.1007/s11705-021-2103-5.
[14] K. Wang, W. Fu, X.-m. Wang, C. Xu, Y. Gao, Y. Liu, X. Zhang, X. Huang, Molecular design of the polyamide layer structure of nanofiltration membranes by sacrificing hydrolyzable groups toward enhanced separation performance, Environ. Sci. Technol. 56 (24) (2022) 17955–17964, https://doi.org/10.1021/acs.est.2c04232.
[15] R. Lo, A. Bhattacharya, B. Ganguly, Probing the selective salt rejection behavior of thin film composite membranes: a DFT study, J. Membr. Sci. 436 (2013) 90–96, https://doi.org/10.1016/j.memsci.2013.02.025.
[16] J. Lee, Y. Shin, C. Boo, S. Hong, Performance, limitation, and opportunities of acid-resistant nanofiltration membranes for industrial wastewater treatment, J. Membr. Sci. 666 (2023) 121142, https://doi.org/10.1016/j.memsci.2022.121142.
[17] D. Dolar, K. Košutić, D. Ašperger, Influence of adsorption of pharmaceuticals onto RO/NF membranes on their removal from water, Water, Air, Soil Pollut. 224 (1) (2012), https://doi.org/10.1007/s11270-012-1377-0.

[18] J. Zhu, J. Hou, R. Zhang, S. Yuan, J. Li, M. Tian, P. Wang, Y. Zhang, A. Volodin, B. Van der Bruggen, Rapid water transport through controllable, ultrathin polyamide nanofilms for high-performance nanofiltration, J. Mater. Chem. A 6 (32) (2018) 15701–15709, https://doi.org/10.1039/c8ta05687k.
[19] Z. Jiang, S. Karan, A.G. Livingston, Water transport through ultrathin polyamide nanofilms used for reverse osmosis, Adv. Mater. 30 (15) (2018) 1705973, https://doi.org/10.1002/adma.201705973.
[20] S.-J. Park, W. Choi, S.-E. Nam, S. Hong, J.S. Lee, J.-H. Lee, Fabrication of polyamide thin film composite reverse osmosis membranes via support-free interfacial polymerization, J. Membr. Sci. 526 (2017) 52–59, https://doi.org/10.1016/j.memsci.2016.12.027.
[21] S. Karan, Z. Jiang, A.G. Livingston, Sub–10 nm polyamide nanofilms with ultrafast solvent transport for molecular separation, Science 348 (6241) (2015) 1347–1351, https://doi.org/10.1126/science.aaa5058.
[22] G. Sauerbrey, Verwendung von Schwingquarzen zur Wägung dünner Schichten und zur Mikrowägung, Z. Phys. 155 (2) (1959) 206–222, https://doi.org/10.1007/BF01337937.
[23] X. Zhang, D.G. Cahill, O. Coronell, B.J. Mariñas, Absorption of water in the active layer of reverse osmosis membranes, J. Membr. Sci. 331 (1–2) (2009) 143–151, https://doi.org/10.1016/j.memsci.2009.01.027.
[24] Y. Li, X. You, R. Li, Y. Li, C. Yang, M. Long, R. Zhang, Y. Su, Z. Jiang, Loosening ultrathin polyamide nanofilms through alkali hydrolysis for high-permselective nanofiltration, J. Membr. Sci. 637 (2021) 119623, https://doi.org/10.1016/j.memsci.2021.119623.
[25] W. Li, R. Zhang, C. Yang, Z. Wang, J. Guan, Y. Li, J. Shen, Y. Su, Z. Jiang, Perfluorooctanoyl chloride engineering toward high-flux antifouling polyamide nanofilms for desalination, J. Membr. Sci. 644 (2022) 120166, https://doi.org/10.1016/j.memsci.2021.120166.
[26] M. Esmaeili, S.H. Mansoorian, A. Gheshlaghi, F. Rekabdar, Performance and morphology evaluation of thin film composite polyacrylonitrile/polyamide nanofiltration membranes considering the reaction time, J. Water Chem. Technol. 40 (4) (2018) 219–227, https://doi.org/10.3103/S1063455X18040070.
[27] F.A. Pacheco, I. Pinnau, M. Reinhard, J.O. Leckie, Characterization of isolated polyamide thin films of RO and NF membranes using novel TEM techniques, J. Membr. Sci. 358 (1–2) (2010) 51–59, https://doi.org/10.1016/j.memsci.2010.04.032.
[28] T.E. Culp, B. Khara, K.P. Brickey, M. Geitner, T.J. Zimudzi, J.D. Wilbur, S.D. Jons, A. Roy, M. Paul, B. Ganapathysubramanian, A.L. Zydney, M. Kumar, E.D. Gomez, Nanoscale control of internal inhomogeneity enhances water transport in desalination membranes, Science 371 (6524) (2021) 72–75, https://doi.org/10.1126/science.abb8518.
[29] V. Freger, S. Srebnik, Mathematical model of charge and density distributions in interfacial polymerization of thin films, J. Appl. Polym. Sci. 88 (5) (2003) 1162–1169, https://doi.org/10.1002/app.11716.
[30] X. Jin, C.Y. Tang, Y. Gu, Q. She, S. Qi, Boric acid permeation in forward osmosis membrane processes: modeling, experiments, and implications, Environ. Sci. Technol. 45 (6) (2011) 2323–2330, https://doi.org/10.1021/es103771a.
[31] L. Lin, R. Lopez, G.Z. Ramon, O. Coronell, Investigating the void structure of the polyamide active layers of thin-film composite membranes, J. Membr. Sci. 497 (2016) 365–376, https://doi.org/10.1016/j.memsci.2015.09.020.
[32] L. Lin, C. Feng, R. Lopez, O. Coronell, Identifying facile and accurate methods to measure the thickness of the active layers of thin-film composite membranes – a comparison of seven characterization techniques, J. Membr. Sci. 498 (2016) 167–179, https://doi.org/10.1016/j.memsci.2015.09.059.
[33] K. Košutić, L. Kaštelan-Kunst, B. Kunst, Porosity of some commercial reverse osmosis and nanofiltration polyamide thin-film composite membranes, J. Membr. Sci. 168 (1) (2000) 101–108, https://doi.org/10.1016/S0376-7388(99)00309-9.
[34] K. Košutić, B. Kunst, RO and NF membrane fouling and cleaning and pore size distribution variations, Desalination 150 (2) (2002) 113–120, https://doi.org/10.1016/S0011-9164(02)00936-0.
[35] G.T. Gray, J.R. McCutcheon, M. Elimelech, Internal concentration polarization in forward osmosis: role of membrane orientation, Desalination 197 (1) (2006) 1–8, https://doi.org/10.1016/j.desal.2006.02.003.
[36] T.Y. Cath, A.E. Childress, M. Elimelech, Forward osmosis: principles, applications, and recent developments, J. Membr. Sci. 281 (1) (2006) 70–87, https://doi.org/10.1016/j.memsci.2006.05.048.
[37] F. Wang, Z. Yang, C.Y. Tang, Modeling water transport in interlayered thin-film nanocomposite membranes: gutter effect vs funnel effect, ACS EST Eng. 2 (11) (2022) 2023–2033, https://doi.org/10.1021/acsestengg.2c00133.
[38] Z. Yang, F. Wang, H. Guo, L.E. Peng, X.-h. Ma, X.-x. Song, Z. Wang, C.Y. Tang, Mechanistic insights into the role of polydopamine interlayer toward improved separation performance of polyamide nanofiltration membranes, Environ. Sci. Technol. 54 (18) (2020) 11611–11621, https://doi.org/10.1021/acs.est.0c03589.
[39] X. Zhu, Z. Yang, Z. Gan, X. Cheng, X. Tang, X. Luo, D. Xu, G. Li, H. Liang, Toward tailoring nanofiltration performance of thin-film composite membranes: novel insights into the role of poly(vinyl alcohol) coating positions, J. Membr. Sci. 614 (2020) 118526, https://doi.org/10.1016/j.memsci.2020.118526.
[40] P. Cheng, Y. Liu, X. Wei, K. Fan, S. Xia, Distinct efficacies of interlayers in tailoring polyamide nanofiltration membrane performance for organic micropollutant removal: dependent on substrate characteristics, Environ. Sci. Technol. 58 (31) (2024) 14022–14033, https://doi.org/10.1021/acs.est.4c04648.
[41] Y. Zong, Q. Long, L. Chen, A. Samadi, H. Luo, K. Liang, X. Wan, F. Liu, Y. Chen, Z. Zhang, S. Zhao, Dual 2D nanosheets with tunable interlayer spacing enable high-performance self-cleaning thin-film composite membrane, J. Membr. Sci. 693 (2024) 122328, https://doi.org/10.1016/j.memsci.2023.122328.
[42] L. Long, C. Wu, Z. Yang, C.Y. Tang, Carbon nanotube interlayer enhances water permeance and antifouling performance of nanofiltration membranes: mechanisms and experimental evidence, Environ. Sci. Technol. 56 (4) (2022) 2656–2664, https://doi.org/10.1021/acs.est.1c07332.
[43] Y. Hu, F. Wang, Z. Yang, C.Y. Tang, Modeling nanovoid-enhanced water permeance of thin film composite membranes, J. Membr. Sci. 675 (2023) 121555, https://doi.org/10.1016/j.memsci.2023.121555.
[44] G.Z. Ramon, M.C.Y. Wong, E.M.V. Hoek, Transport through composite membrane, part 1: is there an optimal support membrane? J. Membr. Sci. 415–416 (2012) 298–305, https://doi.org/10.1016/j.memsci.2012.05.013.
[45] Y. Hu, P. Sarkar, L.E. Peng, F. Wang, Z. Yang, C.Y. Tang, Design ultrathin polyamide membranes against funnel effect: a novel zone-of-influence-based approach, Environ. Sci. Technol. (2025), https://doi.org/10.1021/acs.est.5c01365.
[46] D. Chen, J.R. Werber, X. Zhao, M. Elimelech, A facile method to quantify the carboxyl group areal density in the active layer of polyamide thin-film composite membranes, J. Membr. Sci. 534 (2017) 100–108, https://doi.org/10.1016/j.memsci.2017.04.001.
[47] X.-H. Ma, Z.-K. Yao, Z. Yang, H. Guo, Z.-L. Xu, C.Y. Tang, M. Elimelech, Nanofoaming of polyamide desalination membranes to tune permeability and selectivity, Environ. Sci. Technol. Lett. 5 (2) (2018) 123–130, https://doi.org/10.1021/acs.estlett.8b00016.
[48] Y. Gao, Y. Zhao, X.-m. Wang, C. Tang, X. Huang, Asymmetry of the active layer in pursuit of nanofiltration selectivity via differentiating interfacial reactions of piperazine, Environ. Sci. Technol. 56 (19) (2022) 14038–14047, https://doi.org/10.1021/acs.est.2c04124.
[49] X.-H. Ma, Z. Yang, Z.-K. Yao, H. Guo, Z.-L. Xu, C.Y. Tang, Interfacial polymerization with electrosprayed microdroplets: toward controllable and ultrathin polyamide membranes, Environ. Sci. Technol. Lett. 5 (2) (2018) 117–122, https://doi.org/10.1021/acs.estlett.7b00566.
[50] M.R. Chowdhury, J. Steffes, B.D. Huey, J.R. McCutcheon, 3D printed polyamide membranes for desalination, Science 361 (6403) (2018) 682–685, https://doi.org/10.1126/science.aar2122.